Article

3D-Printed Microcubes for Catalase Drug Delivery

Sungmun Lee,* Dong-Wook Lee, Nitul Rajput, Tadzio Levato, Aya Shanti, and Tae-Yeon Kim

Cite This: *ACS Omega* 2023, 8, 26775−26781

Read Online

| ACCESS | | Metrics & More | | Article Recommendations | | Supporting Information |

ABSTRACT: Oxidative stress, i.e., excessive production of reactive oxygen species (ROS), plays an important role in the pathogenesis of inflammatory diseases such as cardiovascular diseases, cancer, and neurodegenerative diseases. Catalase, an antioxidant enzyme, has great therapeutic potential; however, its efficacy is limited by its delivery to target cells or tissues. In order to achieve efficient delivery, consistent drug distribution, and drug activity, small and uniformly sized drug delivery vehicles are needed. Here, three-dimensional (3D) microcubes were printed by Nanoscribe Photonic Professional GT2, a high-resolution 3D printer, and the characteristics of 3D-printed microcubes as drug delivery vehicles for the delivery of catalase were investigated. The size of the 3D-printed microcubes was 800 nm in length of a square and 600 nm in height, which is suitable for targeting macrophages passively. Microcubes were also tunable in shape and size, and high-resolution 3D printing could provide microparticles with little variation in shape and size. Catalase was loaded on 3D-printed microcubes by nonspecific adsorption, and catalase on 3D-printed microcubes (CAT−MC) retained $83.1 \pm 1.3\%$ activity of intact catalase. CAT−MC also saved macrophages, RAW 264.7, from the cytotoxicity of H_2O_2 by $86.4 \pm 4.1\%$. As drug delivery vehicles, 3D-printed microparticles are very promising due to their small and uniform size, which provides consistent drug distribution and drug activity. Therefore, we anticipate numerous applications of 3D-printed microparticles for delivering therapeutic proteins.
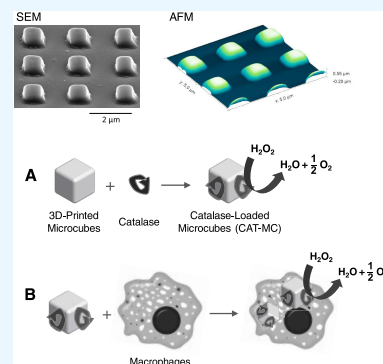
INTRODUCTION

Oxidative stress, i.e., overproduction of reactive oxygen species (ROS), triggers inflammation and it can cause many chronic inflammatory diseases such as diabetes, cancer, neurodegenerative diseases, and cardiovascular diseases.[1,2] ROS are highly reactive oxygen chemicals such as superoxide ($O_2^{\bullet-}$), hydrogen peroxide (H_2O_2), singlet oxygen ($^1O_2$), and hydroxyl radical ($HO^\bullet$).[3,4] ROS are produced as byproducts of normal cellular metabolism, and they are useful tools to destroy biological pathogens.[3,4] Compared to other ROS, H_2O_2 is a relatively mild and stable ROS, and it can act as a signaling molecule or a mediator of apoptotic cell death.[5] However, the overproduction of H_2O_2 deteriorates both mitochondrial membrane structures and function. In physiological systems, antioxidant enzymes such as superoxide dismutase (SOD), glutathione peroxidase, and catalase can deactivate or scavenge ROS. Catalase (EC 1.11.1.6) can decompose H_2O_2 into nontoxic water (H_2O) and oxygen (O_2).[6−8] Catalase can protect cells from apoptosis induced by H_2O_2, and it has great therapeutic potential for the treatment of inflammatory diseases.[9] However, catalase and other therapeutic proteins are not membrane permeable, and therefore, they require effective drug delivery systems to enhance their activity.

Therapeutic proteins such as catalase are highly specific and very active, and they have several advantages over small-molecule drugs;[10] however, most therapeutic proteins require delivery systems to enhance their drug efficacy. There are several delivery methods to minimize the limitations of

therapeutic proteins. The conjugation of poly(ethylene glycol) (PEG) to therapeutic proteins can enhance the retention of therapeutic proteins due to no or very weak immunogenicity.[11,12] Therapeutic proteins can also be encapsulated and protected in nanocolloidal systems using liposomes or other lipid nanocarriers.[13,14] Microparticles using synthetic or natural polymers are also widely used to deliver therapeutic proteins.[15] They can alter the pharmacokinetics and enhance the efficacy of therapeutic proteins. For example, swelling of alginate, one of the hydrogels, microparticles depends on the pH, and therapeutic proteins are released from alginate microparticles at alkaline pH. Zein, one of the natural prolamin proteins, can protect catalase and superoxide dismutase (SOD), antioxidant enzymes, from the harsh conditions of the gastrointestinal (GI) tract, and it enhances their enzymatic activities by targeting activated macrophages.[16,17]

As smart drug delivery systems, stimuli-responsive polymers can also be used for the delivery of therapeutic proteins.[18] Temperature-responsive microparticles are one of the most important groups in smart drug delivery systems.[19] Some polymers or hydrogels experience phase changes from gel to

sol or from sol to gel as temperature increases. Temperature-responsive hydrogels include poly(N,N-diethyl acrylamide) (PDEAM) and poly(N-isopropylacrylamide) (PNIPAM).[20,21] For example, PNIPAM is mixed with therapeutic proteins in an aqueous solution at 32 °C, the lower critical solution temperature (LCST) or below LCST. When they are placed at a body temperature of 37 °C, PNIPAM becomes stronger (sol-to-gel transition), and the therapeutic drugs are released.

Three-dimensional (3D) printing has become a popular technique to fabricate 3D structures using various materials, such as metals, ceramics, and polymers.[22] Due to the diversity of materials and printing methods, 3D printing technology has been developed in the industry and academic areas. The biomedical applications of 3D printing are widespread, covering implants, pharmaceuticals, biosensors, and optics.[23−25] 3D printing technology has been extensively explored, especially in the drug delivery area, since the FDA approved the first 3D-printed tablet Spritam.[23,26] There are several advantages of 3D-printed drug delivery systems over other delivery systems. 3D printing can easily develop diverse geometries and sizes of delivery systems through computer-aided design, which will be useful for controlled and targeted drug release. Therefore, 3D-printed drug delivery systems can be applied to various types of diseases and patients. Eventually, 3D printing technology will be suitable for personalized medicines,[27] and it will be more effective if the amount of dose, dosage form, and drug release is controlled.

Here, a high-resolution 3D printer was used to fabricate microcubes for drug delivery applications. Catalase, a therapeutic protein, was then loaded on 3D-printed microcubes (CAN-MC), and we will investigate how efficiently CAT−MC can decompose H_2O_2 and save macrophages from the cytotoxicity of H_2O_2.

■ MATERIALS AND METHODS

Preparation of 3D-Printed Microcubes. The microcubes were fabricated by three-dimensional two-photon polymerization lithography on a fused silica substrate. A commercial femtosecond laser-based lithography system (Photonic Professional GT2, Nanoscribe) was used with a negative-tone photoresist (IP-Dip2, Nanoscribe). A 63× objective with NA = 1.4 was used to achieve a lateral resolution of approximately 200 nm. Standard dip-in laser lithography (DiLL) mode is applied in this work. The microcubes were designed using computer-aided design (CAD) software, SolidWorks (Dassault Systems, France). The CAD models were exported in the STL file format and then imported into computer-aided manufacturing (CAM) software, DeScribe (Nanoscribe GmbH, Germany), to generate the laser writing path code. The hatching (the distance between adjacent lateral lines) and slicing (the distance between vertical layers) distances were both 100 nm. The laser power was set as 40% of the maximum laser power, and the writing speed was set as 10 mm/s. After printing, the sample was placed on an aluminum mount and immersed in propylene glycol monomethyl ether acetate (PGMEA; Sigma-Aldrich) for 20 min and for 2 min in isopropanol. Finally, the sample was dried in air by evaporation. To increase the fabrication output, galvanometer mirror scanning mode was selected. To reduce the stitching errors, the size of the scanning field was limited to 100 μm × 100 μm.

Physical Characterization of Microcubes Using Electron Microscopy. Scanning electron microscopy (SEM) was used for imaging 3D-printed microcubes. A dual beam system Helios 650 manufactured by Thermo Fisher Scientific was used for the imaging as well as for the cutting. The system had 150 × 150 mm high precision, a high stability piezo stage for precise movement. The microscope had a FEG source for high-resolution imaging. The electron column was an Elstar type also integrated with a monochromator (UC) and beam deceleration. The system can provide sub-nm resolution across the whole 1−30 kV range. The through-the-lens (TLD) detector has the highest collection efficiency of secondary electrons (SE). During the SEM imaging, a 5 kV beam voltage and 100 pA beam current were employed. The integrated focused ion beam column was a Tomahawk type that provided the best quality ion performance. The column had differential pumping and TOF correction capability suitable for higher-resolution ion beam imaging, ion beam milling, and ion beam deposition. 30 keV Ga ion was used to deposit a Pt capping layer and make a cut in order to obtain a cross-sectional view of the particles. For the cut, a regular cross section (RCS) and, subsequently, a cleaning cross section (CCS) were used. The Ga-FIB can perform precise cuts, and the SEM can be used for HR electron imaging.

Atomic Force Microscopy (AFM). Atomic force microscopy (AFM) imaging was carried out on the patterns. The experiment was done using an Asylum Research make system (Jupiter XR). The scanning mode was noncontact. The scanned images are shown in Figure S1 of the Supporting Information. For the AFM imaging, we used a Si cantilever with a resonance frequency of 1500 kHz and a tip radius of 10 ± 2 nm.

Fluorescence Labeling of Catalase. In order to measure the loading efficiency of catalase in microcubes and to study the uptake of catalase-loaded microcubes by the cells, catalase was labeled with a fluorescence dye, fluorescein isothiocyanate (FITC). Briefly, catalase was dissolved in a pH 9.0 buffer solution. Next, 50 μL of 10 mg/mL FITC in dimethyl sulfoxide (DMSO) was mixed with 3 mL of 3.3 mg/mL catalase solutions for 4 h at room temperature. The FITC-labeled catalase was separated from unreacted FITC using a PD-10 desalting column, and it was equilibrated in phosphate-buffered saline (PBS) (pH 7.4).

Catalase-Loaded Microcubes (CAT−MC). The 3D-printed microcubes were detached from the surface of the glass by adding 1 mL of deionized water (DIW), and they were dispersed with a vortexer for 3 min to suspend the microcubes into short segments. Various concentrations of FITC-catalase (0.033, 0.067, 0.100, 0.167, 0.267, 0.333, 0.400, 0.500 mg/mL) were mixed with 15,000 microcubes for 24 h. FITC-catalase on microcubes was separated from free FITC-catalase by ultracentrifugation at 12,000 rpm for 3 min. The amount of catalase loaded on the microparticles was determined by the fluorescence of FITC-catalase on microparticles.

$$\text{loading efficiency (\%)} = \frac{\text{fluorescence of FITC catalase on microcubes}}{\text{total fluorescence of FITC catalase}} \times 100\%$$

Determination of Catalase Activity *In Vitro*. Catalase is an enzyme that decomposes H_2O_2 into H_2O and O_2. Catalase activity was measured by the decomposition rate of H_2O_2. A solution containing either free catalase (0.1 mL of 16.6 μg/
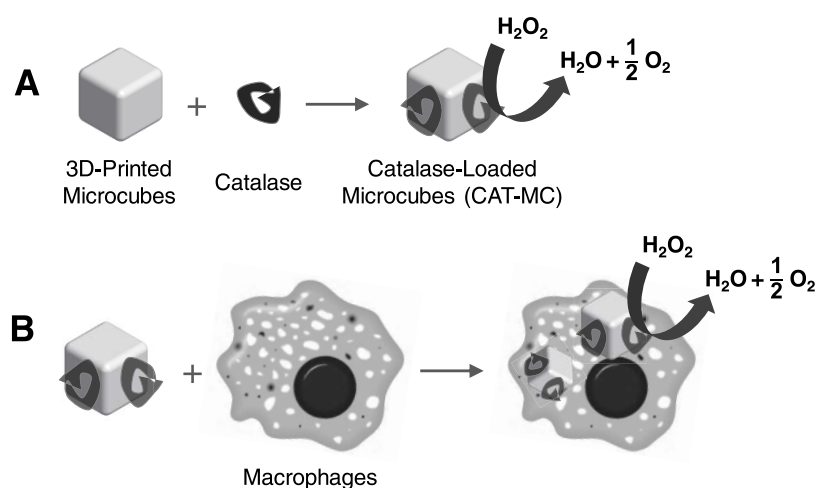
Figure 1. Schematic diagram of catalase-loaded microcubes. (A) The sizes of microcubes printed by the Nanoscribe Photonic Professional GT2 are consistent with little variation. Catalase can be loaded on 3D-printed microcubes by nonspecific adsorption. Catalase on the microcubes has enzymatic activity to decompose hydrogen peroxide (H_2O_2) into water (H_2O) and oxygen (O_2). (B) When catalases on the nanoparticles are taken up by macrophages, they can protect the cells from the cytotoxic H_2O_2 efficiently.

mL) or an equivalent amount of catalase on microcubes was mixed with 2.9 mL of 10 μM H_2O_2 in phosphate buffer (pH 7.4), and the absorbance of H_2O_2 was monitored with time at 240 nm. For comparison, the absorbance of microparticles only (empty microparticles) with H_2O_2 and H_2O_2 only at 240 nm was also monitored.

Cell Culture. RAW 264.7 macrophages (ATCC number: TIB-71), murine macrophage cells from the American Type Culture Collection (ATCC) (Manassas, VA) were cultured at 37 °C under a humidified atmosphere of 5% CO_2 in Dulbecco's modified Eagle's medium (DMEM) containing 10% (v/v) fetal bovine serum (FBS) supplemented with penicillin (100 units/mL) and streptomycin (100 μg/mL).

Cellular Uptake of Catalase-Loaded Microcubes. For the uptake study, RAW 264.7 macrophages were incubated with either 166.7 μg/mL FITC-catalase or an equivalent amount of FITC-catalase-loaded microcubes. At specific time points, the cells were washed three times, and the cellular uptake of catalase-loaded microparticles was measured using an Infinite M200 PRO microplate reader (Tecan, Männedorf, Switzerland) with excitation/emission at 480/520 nm. The uptake was also analyzed by flow cytometry (BD Accuri C6, BD Biosciences) (San Jose, CA) using FITC-catalase.

Cellular Activity Test of CAT−MC-Measurement of Intracellular H_2O_2. RAW 264.7 macrophages were incubated with either 166.7 μg/mL catalase or an equivalent catalase concentration of catalase on microcubes for 4 h. Macrophages were washed with PBS and treated with 100 μM H_2O_2 for 4 h. The cells were washed with PBS three times, trypsinized, and stained with 5 μM 5-(and-6)-chloromethyl-2′,7′-dichlorodihydrofluorescein diacetate, acetyl ester (CM-H_2DCFDA) (Invitrogen, Carlsbad, CA) for measuring H_2O_2. After 20 min, cells were washed three times with ice-cold PBS. The fluorescence of CM-H_2DCFDA was measured by an Infinite M200 PRO microplate reader (Tecan, Männedorf, Switzerland) with excitation/emission at 480/520 nm.

Cell Viability Test (MTT Reduction Assay). A 3-(4,5-dimethylthiazol-2-yl)-2,5-diphenyltetrazolium bromide (MTT) reduction assay was performed to measure the cytotoxicity of H_2O_2 and the activity of catalase. Macrophages (1 × 10^5 cells/well, 96-well plate) in DMEM with 10% FBS were incubated

either with 300 μg/mL catalase or an equivalent catalase concentration of catalase on microcubes for 4 h. Cells were washed three times with medium, and cells were treated with 200 μM H_2O_2 for 24 h. Next, 20 μL of MTT solution (5 mg/mL in PBS) was added to each well, and the cells were incubated for 2 h. Then, 200 μL of DMSO was added to dissolve the resulting formazan crystals. After 10 min of incubation, the absorbance at 570 nm was measured using an Infinite M200 PRO microplate reader (Tecan, Männedorf, Switzerland). The percentage of cell viability was calculated by comparing the absorbance of the control cells to that of H_2O_2 and/or catalase/microcube-treated cells.

$$\text{cell viability } (\%) = \frac{\text{absorbance of cells treated with } H_2O_2 \text{ and/orcatalase}}{\text{absorbance of control cells (media treated only)}} \times 100\%$$

■ RESULTS AND DISCUSSION

Catalase, an antioxidant enzyme, has great therapeutic potential, and it can scavenge the overproduced H_2O_2, one of the reactive oxygen species, which retards or prevents aging-related diseases and disorders such as cardiovascular diseases, cancer, and neurodegenerative diseases. Here, as shown schematically in Figure 1, 3D microcubes were printed to serve as drug delivery vehicles for delivering catalase to macrophages.

The 3D microcubes were printed by a higher-resolution 3D printer, Nanoscribe Photonic Professional GT2. The higher-resolution 3D printer has many advantages over conventional 3D printers. It includes a higher resolution with a good quality print for further processing and fast and flexible design iterations. Catalase was loaded on 3D-printed microcubes by nonspecific adsorption. Both free catalase and catalase on the microcubes decomposed hydrogen peroxide (H_2O_2) into water (H_2O) and oxygen (O_2). When CAT−MC were incubated with macrophages, they were taken up by macrophages, and they protected the cells from the cytotoxic H_2O_2 efficiently.

In order to achieve the goals described in the schematic diagram (Figure 1), microcubes were first printed out by the
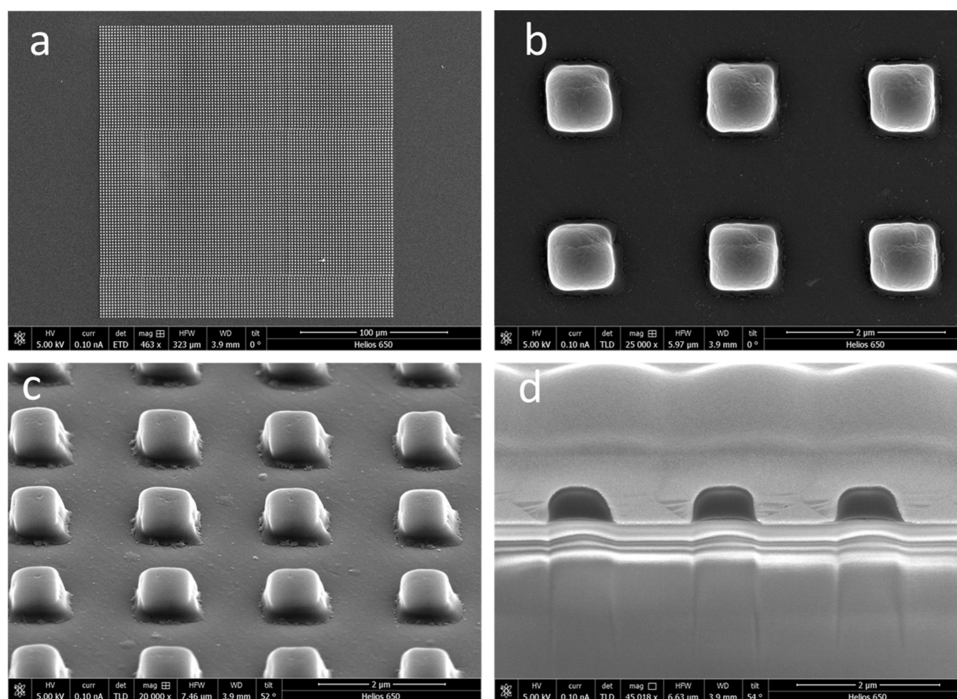
Figure 2. SEM images of the 3D-printed microcubes. (a) and (b) are top-view images of the microcubes, (c) is a tilted view, and (d) is a cross-sectional view of the particles.

Nanoscribe Photonic Professional GT2 to serve as a drug delivery vehicle for delivering catalase.

Figure 2 shows the patterned 3D microcubes imaged by a scanning electron microscope (SEM). The microcubes have retained smooth deposition without any substantial distortion in the shape or size. The matrix shown in the figure is 100 × 100 square particles. The pattern covers a total area of 200 × 200 μm^2. The top view of microcubes has nearly square microparticles with a side length of 0.8 μm or 800 nm, as shown in Figure 2a,b. The 3D printing in Figure 2a,b has a periodicity of 2 μm in both horizontal and vertical directions with an interparticle distance of approximately 1.2 μm. The high-resolution images indicate smooth deposition of the particles without any residue left in between the particles. Figure 2c is a tilted view of the particles that provides an elevated view of the grown particles. Figure 2d is a cross-sectional view of the particles. As mentioned, the particles were deposited with a Pt material on top of them. Then, FIB was used to cut part of the material and extract the cross-sectional images. In the image, the black (low intensity) periodic patterns are the fabricated particles. The image also suggests the smoothness of the surface as well as the high aspect ratio of the square particles. The cross-sectional imaging suggests the height of the particles as 600 nm, which is consistent among all of the deposited particles. Atomic force microscopy (AFM) imaging was also carried out on the patterns. The experiment was done using a noncontact mode in an Asylum Research make system (Jupiter XR). The scanned images are shown in Figure S1 of the Supporting Information. For further experiments, the particles on the glass were collected by adding 1 mL of deionized water to the particles. In Figure S2 of the Supporting Information, the status of particles on the glass was monitored with time after the hydration of particles. The rectangle dark spot of particles (Figure S2A) was getting brighter in 2 min (Figure S2B), which means that all particles

were transferred to water in 5 min. According to the material safety data sheet (MSDS) provided by Nanoscribe, IP-Dip polymers are not water soluble, and therefore, microcubes should be dispersed in water when we add water to them.

In the next step, catalase was loaded on 3D-printed microcubes by nonspecific adsorption. In Figure 3, the amount of catalase was linearly adsorbed on microcubes at or below 0.3 mg/mL; however, it reached a plateau above 0.3 mg/mL. At 0.3 mg/mL catalase concentration, the loading efficiency of
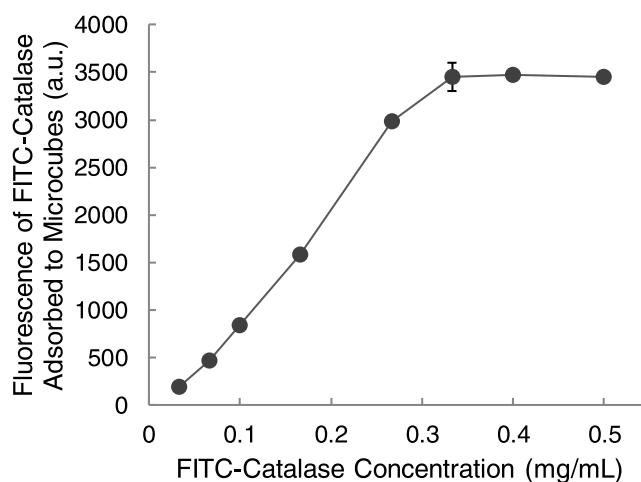
Figure 3. Loading FITC-catalase on the 3D-printed microcubes. For easy quantification, catalase was labeled with FITC, a fluorescent dye. Various concentrations of FITC-catalase were incubated with 15,000 microcubes for 24 h. FITC-catalase loaded on microcubes was separated from free FITC-catalase by ultracentrifugation at 12,000 rpm for 3 min. The amount of catalase loaded on the microcubes, or the loading efficiency, was determined by the fluorescence of FITC-catalase on microcubes. ($n = 3$, error bar = mean ± standard deviation).
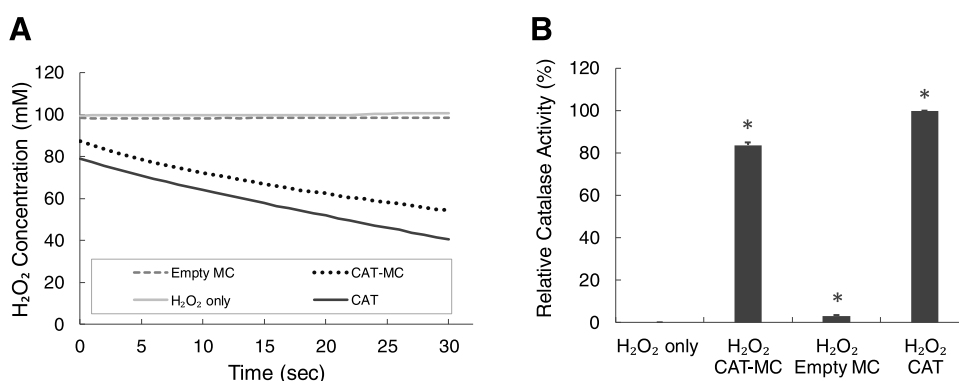
Figure 4. Enzyme activity of catalase on 3D-printed microcubes *in vitro* catalase activity was determined by measuring the reduction rate of H_2O_2. (A) Decomposition of H_2O_2 was monitored with time at 240 nm. (B) Significance of the results was determined via the *t*-test compared to H_2O_2 only with $*p < 0.05$. ($n = 3$, error bar = mean $\pm$ standard deviation) (CAT: catalase, MC: microcubes, and CAT−MC: catalase on 3D-printed microcubes).
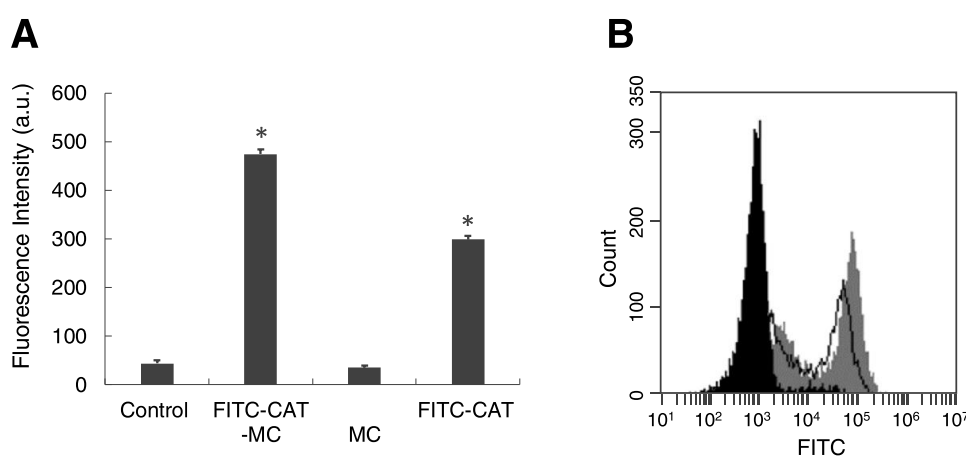
Figure 5. 3D-printed microcubes can enhance the uptake of catalase by macrophages *in vitro*. (A) Cellular uptake of the FITC-catalase by macrophages was detected *in vitro*. Fluorescence of FITC-catalase was measured by an Infinite M200 PRO microplate reader ($n = 3$, error bar = mean $\pm$ standard deviation). (B) Flow cytometer detected macrophages only (black-filled shade) or macrophages treated by FITC-catalase (black line) or macrophages treated by FITC-catalase on 3D-printed microcubes (gray-filled shade).

catalase on 3D-printed microcubes was 18.0 $\pm$ 0.8% (mean $\pm$ standard deviation) in 24 h of incubation.

The graph showed a typical Langmuir adsorption isotherm, which demonstrated the adsorption of the adsorbate, catalase, on the surface of the adsorbent, 3D-printed microcubes. The Langmuir adsorption isotherm assumes that the adsorbate creates only a monolayer on the adsorbent's surface. It refers to the equilibrium between the adsorbent and the adsorbate system. Adsorption of catalase on microcubes is very consistent, and the adsorbed amount of catalase on microcubes is almost the same at a specific concentration of catalase and microcubes. The percentage standard deviation at each data point is 1.45 $\pm$ 1.44% demonstrating very small error bars in Figure 3. The very small error bars in adsorption resulted from the small variation in the size of microcubes. This is an advantage of the 3D printing method over other methods to formulate drug delivery vehicles such as microcubes.

In Figure 4, the activity of catalase on 3D-printed microcubes was investigated. Catalase activity was determined by measuring the reduction rate of H_2O_2. In Figure 4A, H_2O_2 was incubated with either free catalase or catalase on microcubes, and the decomposition of H_2O_2 was monitored with time. As shown in Figure 4B, catalase on 3D-printed microcubes retained 83.1 $\pm$ 1.3% activity of intact free catalase.

The decrease of catalase activity may result from the hydrophobic interaction between catalase and microcubes during the catalase loading on microcubes. Proteins are unfolded or denatured when they are exposed to hydrophobic environments. IP-Dip polymers provide a hydrophobic environment, and catalase might lose its activity when it comes in contact with IP-Dip polymers. However, catalase on microcubes maintained more activity than the activity of catalase on other hydrophobic drug delivery vehicles.[28] For example, catalase in hydrophobic carbon-based materials such as graphene oxide retained only 40−60% activity of intact catalase.[28]

In inflammatory diseases, activated macrophages markedly increase reactive oxygen species (ROS) that cause all pathophysiological features of inflammatory diseases. Activated macrophages are a major target for anti-inflammatory therapy. We performed experiments to determine if the 3D-printed microcubes could enhance the delivery of catalase into macrophages. For the uptake study, catalase was labeled with a fluorescence dye, FITC, and the FITC-catalase loaded on 3D-printed microparticles was incubated with macrophages (RAW 264.7). The uptake of catalase by cells is then measured by a fluorescence microplate reader (Figure 5A) and flow cytometry (Figure 5B). Figure 5 demonstrates that the uptake
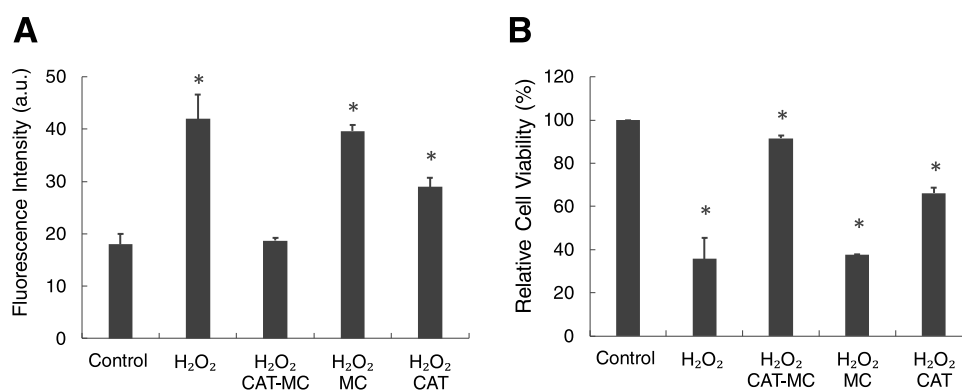
Figure 6. Catalase-loaded microcubes protect macrophages from the toxicity of H_2O_2. Macrophages were incubated with either catalase-loaded microcubes or free catalase. (A) The intracellular level of H_2O_2 and (B) cellular toxicities were measured. For statistical analysis, three independent wells were measured for each sample. Significance of the results was determined via the t-test compared to cells only (control) with *$p < 0.05$. Error bar = mean $\pm$ standard deviation.

of the FITC-catalase loaded on 3D-printed microparticles by macrophages was much enhanced compared to the uptake of the FITC-catalase only. IP-Dip has also autofluorescence at an excitation wavelength of 480 nm and an emission wavelength of 520 nm.

In Figure S3A of the Supporting Information, fluorescence microscopy images demonstrated that microcubes also showed fluorescence; however, the fluorescence level of microcubes is not strong compared to the fluorescence of FITC in Figure S3B of the Supporting Information. Therefore, the autofluorescence of IP-Dip was not considered in the analysis of the uptake study, and only the fluorescence of FITC-catalase was used for the uptake analysis in Figure 5.

Next, we investigated if CAT—MC in macrophages can scavenge H_2O_2 in vitro. Figure 6 demonstrates that CAT—MC in macrophages can scavenge H_2O_2 efficiently, and they can protect macrophages from the cytotoxicity of H_2O_2. RAW 264.7 macrophages were incubated with free catalase or an equivalent catalase on microcubes (CAT—MC) for 4 h. Cells were washed with PBS, and they were treated with 200 μM H_2O_2 for 24 h. Free catalase by itself scavenged H_2O_2 of macrophages by $53.8 \pm 7.3\%$ compared to the H_2O_2 level without catalase, whereas CAT—MC removed most of the H_2O_2 by $96.8 \pm 6.5\%$ (Figure 6A), which was the same H_2O_2 level as the H_2O_2 level of the control group (no H_2O_2 treatment). CAT—MC also protected macrophages from the toxicity caused by H_2O_2 more efficiently (Figure 6B). CAT—MC saved the cells by $86.4 \pm 4.1\%$. From Figures 5 and 6, the activity of CAT—MC was enhanced by the increased uptake of microcubes by macrophages.

In conclusion, we applied 3D microcubes printed by a Nanoscribe Photonic Professional GT2 to the drug delivery of catalase. 3D-printed microcubes are uniform in size compared to particles prepared by other polymeric particle formations, which resulted in very small error bars in drug loading, drug activities, and cell culture experiments in vitro. Based on the results, we anticipate numerous applications of 3D-printed microcubes in drug delivery due to easy fabrication, small and uniform size, tunable size, and enhanced cellular uptake.

ASSOCIATED CONTENT

Supporting Information

The Supporting Information is available free of charge at https://pubs.acs.org/doi/10.1021/acsomega.3c00789.

AFM images of the patterned nanotubes (Figure S1); morphological structure of 3D-printed nanotubes (Figure S2); and autofluorescence of 3D-printed nanoparticles (Figure S3) (PDF)

AUTHOR INFORMATION

Corresponding Author

Sungmun Lee — *Department of Biomedical Engineering, Khalifa University of Science and Technology, Abu Dhabi 127788, UAE; Healthcare Engineering Innovation Center, Khalifa University of Science and Technology, Abu Dhabi 127788, UAE;* ⓞ orcid.org/0000-0002-1699-8376; Phone: +971 2 312 3945; Email: sung.lee@ku.ac.ae

Authors

Dong-Wook Lee — *Advanced Materials Research Center, Technology Innovation Institute, Abu Dhabi 9639, UAE*
Nitul Rajput — *Advanced Materials Research Center, Technology Innovation Institute, Abu Dhabi 9639, UAE*
Tadzio Levato — *Advanced Materials Research Center, Technology Innovation Institute, Abu Dhabi 9639, UAE*
Aya Shanti — *Healthcare Engineering Innovation Center and Department of Biology, Khalifa University of Science and Technology, Abu Dhabi 127788, UAE*
Tae-Yeon Kim — *Department of Civil Infrastructure and Environmental Engineering, Khalifa University of Science and Technology, Abu Dhabi 127788, UAE*

Complete contact information is available at:
https://pubs.acs.org/10.1021/acsomega.3c00789

Notes

The authors declare no competing financial interest.

REFERENCES

(1) Forman, H. J.; Zhang, H. Targeting oxidative stress in disease: promise and limitations of antioxidant therapy. *Nat. Rev. Drug Discovery* **2021**, *20*, 689−709.

(2) Uttara, B.; Singh, A. V.; Zamboni, P.; Mahajan, R. T. Oxidative stress and neurodegenerative diseases: a review of upstream and

downstream antioxidant therapeutic options. *Curr. Neuropharmacol.* **2009**, *7*, 65−74.

(3) Collin, F. Chemical Basis of Reactive Oxygen Species Reactivity and Involvement in Neurodegenerative Diseases. *Int. J. Mol. Sci.* **2019**, *20*, No. 2407.

(4) Li, Y. R.; Jia, Z.; Trush, M. A. Defining ROS in Biology and Medicine. *React. Oxygen Species* **2016**, *1*, 9−21.

(5) Milkovic, L.; Cipak Gasparovic, A.; Cindric, M.; Mouthuy, P. A.; Zarkovic, N. Short Overview of ROS as Cell Function Regulators and Their Implications in Therapy Concepts. *Cells* **2019**, *8*, No. 793.

(6) He, L.; He, T.; Farrar, S.; Ji, L.; Liu, T.; Ma, X. Antioxidants Maintain Cellular Redox Homeostasis by Elimination of Reactive Oxygen Species. *Cell. Physiol. Biochem.* **2017**, *44*, 532−553.

(7) Kelly, F. J.; Cotgrove, M.; Mudway, I. S. Respiratory tract lining fluid antioxidants: the first line of defence against gaseous pollutants. *Cent. Eur. J. Public Health* **1996**, *4*, 11−14.

(8) MatÈs, J. M.; Perez-Gomez, C.; Nunez de Castro, I. Antioxidant enzymes and human diseases. *Clin. Biochem.* **1999**, *32*, 595−603.

(9) Nandi, A.; Yan, L. J.; Jana, C. K.; Das, N. Role of Catalase in Oxidative Stress- and Age-Associated Degenerative Diseases. *Oxid. Med. Cell. Longevity* **2019**, *2019*, No. 9613090.

(10) Leader, B.; Baca, Q. J.; Golan, D. E. Protein therapeutics: a summary and pharmacological classification. *Nat. Rev. Drug Discovery* **2008**, *7*, 21−39.

(11) Banerjee, S. S.; Aher, N.; Patil, R.; Khandare, J. Poly(ethylene glycol)-Prodrug Conjugates: Concept, Design, and Applications. *J. Drug Delivery* **2012**, *2012*, No. 103973.

(12) Jevsevar, S.; Kunstelj, M.; Porekar, V. G. PEGylation of therapeutic proteins. *Biotechnol. J.* **2010**, *5*, 113−128.

(13) Hou, X.; Zaks, T.; Langer, R.; Dong, Y. Lipid nanoparticles for mRNA delivery. *Nat. Rev. Mater.* **2021**, *6*, 1078−1094.

(14) Martins, S.; Sarmento, B.; Ferreira, D. C.; Souto, E. B. Lipid-based colloidal carriers for peptide and protein delivery–liposomes versus lipid nanoparticles. *Int. J. Nanomed.* **2007**, *2*, 595−607.

(15) George, A.; Shah, P. A.; Shrivastav, P. S. Natural biodegradable polymers based nano-formulations for drug delivery: A review. *Int. J. Pharm.* **2019**, *561*, 244−264.

(16) Lee, S.; Alwahab, N. S.; Moazzam, Z. M. Zein-based oral drug delivery system targeting activated macrophages. *Int. J. Pharm.* **2013**, *454*, 388−393.

(17) Lee, S.; Kim, Y. C.; Park, J. H. Zein-alginate based oral drug delivery systems: Protection and release of therapeutic proteins. *Int. J. Pharm.* **2016**, *515*, 300−306.

(18) Lu, Y.; Sun, W.; Gu, Z. Stimuli-responsive nanomaterials for therapeutic protein delivery. *J. Controlled Release* **2014**, *194*, 1−19.

(19) Karimi, M.; Sahandi Zangabad, P.; Ghasemi, A.; Amiri, M.; Bahrami, M.; Malekzad, H.; Ghahramanzadeh Asl, H.; Mahdieh, Z.; Bozorgomid, M.; Ghasemi, A.; et al. Temperature-Responsive Smart Nanocarriers for Delivery Of Therapeutic Agents: Applications and Recent Advances. *ACS Appl. Mater. Interfaces* **2016**, *8*, 21107−21133.

(20) Haq, M. A.; Su, Y.; Wang, D. Mechanical properties of PNIPAM based hydrogels: A review. *Mater. Sci. Eng., C* **2017**, *70*, 842−855.

(21) Xu, X.; Liu, Y.; Fu, W.; Yao, M.; Ding, Z.; Xuan, J.; Li, D.; Wang, S.; Xia, Y.; Cao, M. Poly(N-isopropylacrylamide)-Based Thermoresponsive Composite Hydrogels for Biomedical Applications. *Polymers* **2020**, *12*, No. 580.

(22) Arefin, A. M. E.; Khatri, N. R.; Kulkarni, N.; Egan, P. F. Polymer 3D Printing Review: Materials, Process, and Design Strategies for Medical Applications. *Polymers* **2021**, *13*, No. 1499.

(23) Beg, S.; Almalki, W. H.; Malik, A.; Farhan, M.; Aatif, M.; Rahman, Z.; Alruwaili, N. K.; Alrobaian, M.; Tarique, M.; Rahman, M. 3D printing for drug delivery and biomedical applications. *Drug Discovery Today* **2020**, *25*, 1668−1681.

(24) Wang, Q.; Han, G.; Yan, S.; Zhang, Q. 3D Printing of Silk Fibroin for Biomedical Applications. *Materials* **2019**, *12*, No. 504.

(25) Cho, H.; Jammalamadaka, U.; Tappa, K. Nanogels for Pharmaceutical and Biomedical Applications and Their Fabrication Using 3D Printing Technologies. *Materials* **2018**, *11*, No. 302.

(26) Economidou, S. N.; Lamprou, D. A.; Douroumis, D. 3D printing applications for transdermal drug delivery. *Int. J. Pharm.* **2018**, *544*, 415−424.

(27) Vaz, V. M.; Kumar, L. 3D Printing as a Promising Tool in Personalized Medicine. *AAPS PharmSciTech* **2021**, *22*, 49.

(28) Li, Y.; Liao, K.; Lee, S. A comparative study of antioxidant-loaded carbon nanoparticles as drug delivery vehicles. *RSC Adv.* **2014**, *4*, 56992−56997.